Charge density wave in layered $La_{1-x}Ce_xSb_2$

R. F. Luccas,[1,2] A. Fente,[1] J. Hanko,[1] A. Correa-Orellana,[2] E. Herrera,[1] E. Climent-Pascual,[2] J. Azpeitia,[2] T. Pérez-Castañeda,[1] M. R. Osorio,[1] E. Salas-Colera,[3,2] N. M. Nemes,[4] F. J. Mompean,[2,5] M. García-Hernández,[2,5] J. G. Rodrigo,[1,5] M. A. Ramos,[1,5] I. Guillamón,[1,5] S. Vieira,[1,5] and H. Suderow[1,5,*]

[1]*Laboratorio de Bajas Temperaturas, Departamento de Física de la Materia Condensada, Instituto de Ciencia de Materiales Nicolás Cabrera and Condensed Matter Physics Center (IFIMAC), Universidad Autónoma de Madrid, E-28049 Madrid, Spain*

[2]*Instituto de Ciencia de Materiales de Madrid, Consejo Superior de Investigaciones Científicas (ICMM-CSIC), Sor Juana Inés de la Cruz 3, 28049 Madrid, Spain*

[3]*SpLine, Spanish CRG Beamline, European Synchroton Radiation Facility (ESRF), BP220-38042 Grenoble Cedex, France*

[4]*GFMC, Departamento de Física Aplicada III, Universidad Complutense de Madrid, Campus Moncloa, E-28040 Madrid, Spain*

[5]*Unidad Asociada de Bajas Temperaturas y Altos Campos Magnéticos, UAM, CSIC, Campus de Cantoblanco, E-28049 Madrid, Spain*

(Received 9 December 2014; revised manuscript received 15 October 2015; published 29 December 2015)

The layered rare-earth diantimonides RSb_2 are anisotropic metals with generally low electronic densities whose properties can be modified by substituting the rare earth. $LaSb_2$ is a nonmagnetic metal with a low residual resistivity presenting a low-temperature magnetoresistance that does not saturate with the magnetic field. It has been proposed that the latter can be associated to a charge density wave (CDW), but no CDW has yet been found. Here we find a kink in the resistivity above room temperature in $LaSb_2$ (at 355 K) and show that the kink becomes much more pronounced with substitution of La by Ce along the $La_{1-x}Ce_xSb_2$ series. We find signatures of a CDW in x-ray scattering, specific heat, and scanning tunneling microscopy (STM) experiments in particular for $x \approx 0.5$. We observe a distortion of rare-earth–Sb bonds lying in-plane of the tetragonal crystal using x-ray scattering, an anomaly in the specific heat at the same temperature as the kink in resistivity and charge modulations in STM. We conclude that $LaSb_2$ has a CDW which is stabilized in the $La_{1-x}Ce_xSb_2$ series due to substitutional disorder.

DOI: 10.1103/PhysRevB.92.235153 PACS number(s): 72.15.Eb, 71.45.Lr, 75.30.Fv, 61.66.Dk

I. INTRODUCTION

Many rare-earth (R) diantimonide materials (RSb_2) are metals with highly anisotropic properties related to their layered structure. High-quality samples of centimeter sizes with low residual resistivity can be obtained using solution growth [1,2]. RSb_2 crystallize in the orthorhombic $SmSb_2$ structure (Fig. 1). $LaSb_2$ is the only compound in the RSb_2 series showing superconducting properties [2]. These are still unclear, presenting several features that differ from the behavior expected in a simple s-wave BCS superconductor [3–7]. For instance, the superconducting gap is broadened, with states at the Fermi level and the resistive transition is very wide. Above the critical field in the normal phase, the resistivity of $LaSb_2$ increases approximately linearly with the magnetic field up to 45 T when the field is applied along the c axis [2,3]. This is at odds with the usual magnetoresistance behavior of metals, which gives a quadratic field dependence that saturates at high magnetic fields [8,9]. Linear magnetoresistance is of practical interest because of the potential applications connected with unconventional scattering mechanisms under magnetic fields [10]. It has been proposed that the large and positive magnetoresistance might enable making magnetic field sensors out of $LaSb_2$ [3].

Magnetoresistance curves that do not saturate at very high magnetic fields have been recently discussed in quasi-two-dimensional systems. Graphene [11–14], Bi thin films, Dirac semimetals, and topological insulators [15] show large and unsaturating magnetoresistances. Possible explanations involve the linear electronic dispersion relation and quantum conduction [16], low electronic densities or inhomogeneities and disorder [10,17], coherent anisotropic quantum fluctuations [18], and charge density waves (CDWs) [9,19].

CDWs have been reported in $PrSb_2$ and in $LaAgSb_2$. These systems also present, as $LaSb_2$, large and unsaturating magnetoresistances [2]. In $LaAgSb_2$, the CDW was observed in thermodynamic and transport measurements, in x-ray scattering experiments, and studied as a function of substitution [20–22]. Substitution of La with Ce in $La_{1-x}Ce_xAgSb_2$ gives a suppression of the CDW and a broadening of the observed features in resistivity [23,24]. Here we find a kink in the resistivity of $LaSb_2$ above room temperature evidencing CDW order in this compound. We discuss its evolution with substitution of La by Ce. We find that the kink in the resistivity becomes more pronounced with substitutional disorder.

II. EXPERIMENT

Samples of $La_{1-x}Ce_xSb_2$ were grown from excess Sb flux [2,25,26]. Ce, La, and Sb materials (Ce and La from [27] and Sb from Alfa Aesar with 99.9999% purity) were put together in an alumina crucible and sealed in a quartz ampoule in inert He gas atmosphere. Ampoules were heated to 950 °C for 3 hours, cooled down to 650 °C in 70 hours, and finally spun. As a result, we obtained crystals (Fig. 1) with mirror surfaces showing terraces and no visible influence of the substitution on the shape and form of the crystals. Inductively coupled plasma (ICP) mass spectrometry analysis shows Ce substitution values within 5% of the nominal composition. The composition of some samples was further examined by x-ray diffraction at room temperature using a Bruker D8

*Corresponding author: hermann.suderow@uam.es

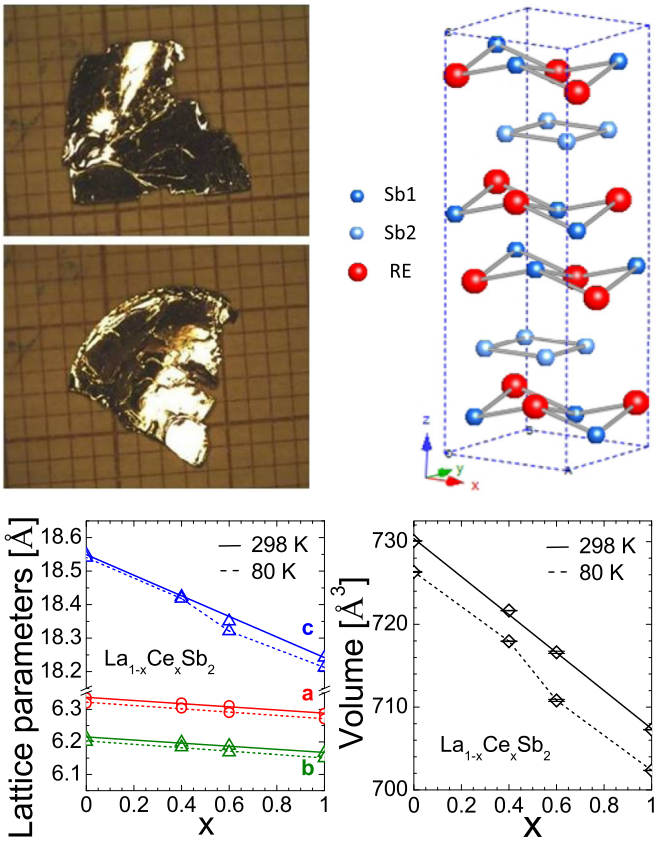

FIG. 1. (Color online) Top panels show pictures of the obtained crystals (left, photographed on millimeter paper) and the crystal structure of $La_{1-x}Ce_xSb_2$ (right). For clarity, we have removed bonds in between planes. In the bottom panels, we show the dependence of the lattice parameters with temperature and Ce content, x (left) and the variation of the unit cell volume with x (right), at room temperature and at liquid nitrogen temperature (for $x = 0,0.4,0.6,1$).

ADVANCE θ-θ diffractometer equipped with a Lynx-Eye detector. To determine the evolution of the c-axis lattice parameter from $(00l)$ reflections we use a Bruker D8 4-circles diffractometer on exfoliated samples with different Ce atomic ratio. A full structural study of selected compositions was performed by the Rietveld method (see Appendix). For this purpose, fine powders were carefully prepared and packed into quartz capillaries 0.4 mm diameter. X-ray powder diffraction (XRPD) data were collected at 80 and 300 K, using an incident energy of 20 keV ($\lambda = 0.621$ Å), at the BM25A station of the SpLine beamline at ESRF in Grenoble. Lattice parameters, atomic positions, and thermal parameters were refined in the space group $Cmca$(#64), using the FullProf program suite [28,29]. Resistivity as a function of temperature and magnetic field was measured in the four-wire configuration in a Quantum Design PPMS system with the current applied along the basal plane of the crystal structure. The magnetic transitions were traced by specific heat measurements using a conventional helium 4 cryostat, and a quasiadiabatic method described in Ref. [30]. Using this method, we did not find any feature indicative of a CDW at higher temperatures. Thus, we implemented an AC microcalorimeter based on a XEN-TCG3880. We thermally short-circuited heating and sensing elements by a 200-nm-thick gold layer to improve samples' thermalization. We measured a sample with about 10 μg mounted using Apiezon grease. To make the STM experiments on best possible surfaces, we started by gluing a piece of brass on top of thin crystals, which we removed at low temperatures by a mechanical setup similar to the ones described in Refs. [31,32]. We prepared in this way ten samples of different concentrations x, but we were unable to obtain reproducible tunneling conditions. Optical inspection after the experiments revealed that this was due to loose layers lying on the surface. Layers in this compound are like aluminum foil, and they easily remain on the surface after cleaving. We were thus forced to use *ex situ* cleaved samples, from which we carefully peeled all layers off at ambient conditions, prior to the STM measurement, leaving surfaces without freestanding layers [4]. Usually, best images were obtained at constant current mode, with a bias voltage of 100 mV and a tunneling resistance of 10 MΩ.

III. RESULTS

The structure of $La_{1-x}Ce_xSb_2$ is typical of the dianti-monides, and is shown in Fig. 1. To a large extent, it can be described as the stacking of R-Sb layers (denoted RSb, where R = La, Ce) and layers composed solely of Sb. The stacking order is RSb-Sb-RSb-RSb-Sb-RSb. Sb1 are the Sb atoms in the RSb planes and Sb2 those in the Sb planes. In Fig. 1 (lower panels) we show the lattice parameters as a function of temperature and Ce concentration. We observe thermal contraction of the lattice and, in addition, a contraction of the lattice from $LaSb_2$ to $CeSb_2$ [33]. We have studied interatomic distances inside RSb and Sb planes (intralayer interatomic distances) as well as between planes (intralayer interatomic distances) at room temperature and at 80 K (Figs. 2 and 3). Near 50% Ce content there is a considerable distortion of the coordination polyhedra within the RSb layers (interlayer distances, Fig. 2). Interatomic distances computed from the polyhedral central atom to atoms laying above or below the

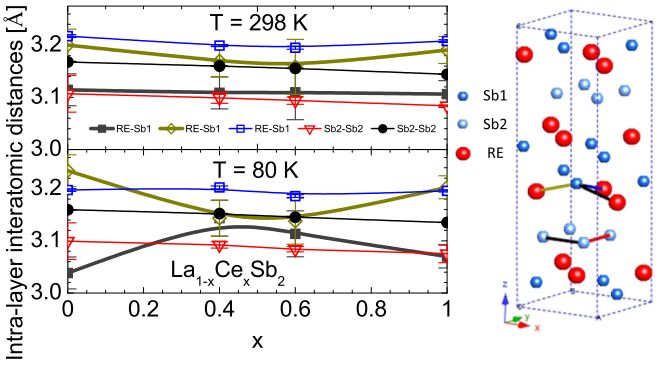

FIG. 2. (Color online) Inter-layer bond distances as a function of x for the $La_{1-x}Ce_xSb_2$ compounds at 80 and 300 K. Lines are guides to the eye. In the right panel we show the crystal structure, and the bonds which we have followed as a function of x and temperature, and which we represent in the left panel (using the same colors). Note that there is a sizable distortion of the inter-layer bonds between rare-earth and Sb atoms when decreasing temperature for intermediate compositions.

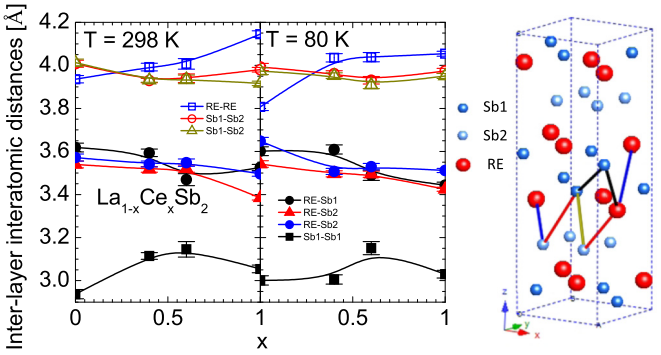

FIG. 3. (Color online) Inter-layer bond distances as a function of x for the $La_{1-x}Ce_xSb_2$ compounds at 80 and 300 K. Lines are guides to the eye. Colors in the left panels correspond to bonds in the representation of the crystal structure on the right. Note that, although generally the volume of the unit cell decreases with x (Fig. 1), there is neither a discernible tendency nor temperature dependence for the out-of-plane behavior of the lattice.

reference layers (interlayer distances, Fig. 3) do not exhibit clear evolutions with x.

In the compound $CeSb_2$ we observe the expected magnetic transitions through specific heat (Fig. 4) and magnetization (see also Appendix) [1,2]. $CeSb_2$ shows a set of three magnetic

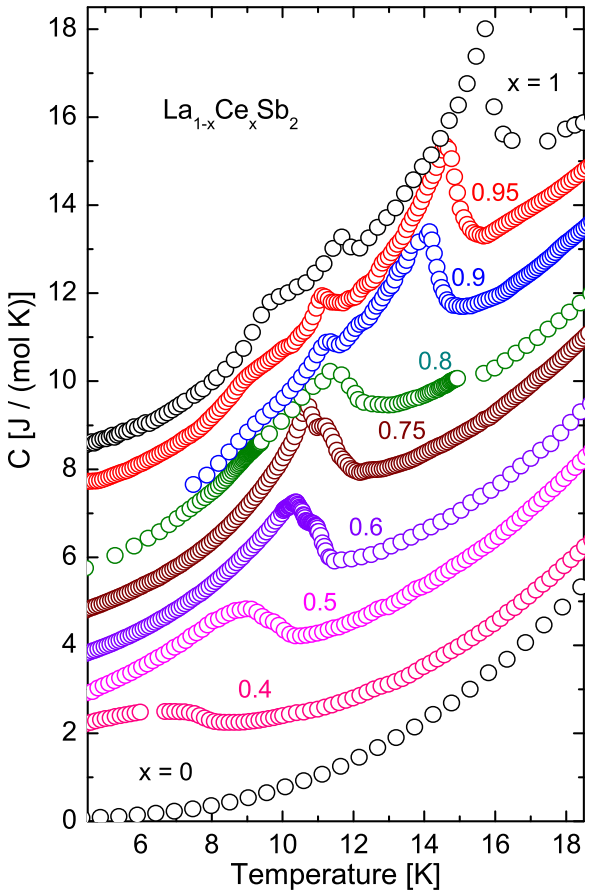

FIG. 4. (Color online) Specific heat vs temperature of $La_{1-x}Ce_xSb_2$ for different x concentrations. The peaks and anomalies correspond to magnetic transitions observed above $x \approx 0.4$.

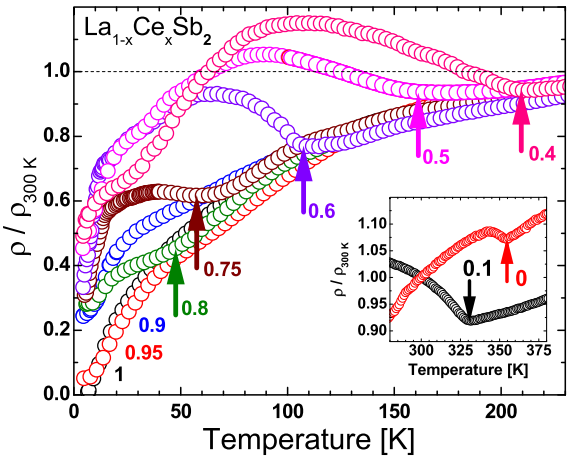

FIG. 5. (Color online) Resistivity as a function of temperature for $x \geqslant 0.4$ normalized to one at 300 K. Note the pronounced kink at the CDW ordering temperature (marked by arrows; numbers are respective concentrations x). The kink becomes smeared when magnetic and CDW transition temperatures become comparable for large x. In the inset, we show the data for $x = 0$ and $x = 0.1$ at higher temperatures. Note that for these concentrations the kink is observed above room temperature.

transitions, starting at $T_C = 16$ K, which evolve continuously when substituting Ce with La. The series of three transitions, the upper λ-like transition at $T_C = 16$ K, the 12 K small λ-like peak, and the shoulder at 9 K are all shifted to lower temperatures, and remain up to a concentration of about $x = 0.8$, where the small 9 K bump is barely visible, and the $T_C = 16$ K and 12 K transitions join into a large two-step-like anomaly. At lower Ce concentrations, the two transitions are still visible, but are strongly smeared, leading to a broad peak at $x = 0.4$, where magnetic order no longer produces a sharp transition.

In Fig. 5 we show the resistivity for $x \geqslant 0.4$ (normalized to the room temperature value) as a function of temperature. For $CeSb_2$ ($x = 1$) we find the same resistivity vs temperature as in previous work [2]. When decreasing the Ce concentration, we find that the low-temperature resistivity (normalized to the room temperature value) increases. There are downturns appearing at temperatures coinciding with the magnetic specific-heat anomalies shown in Fig. 4. These downturns signal the onset of long-range magnetic order. In addition, we observe for $x < 0.9$ a kink with an upturn. This shows the onset of CDW for intermediate concentrations. The kink becomes well developed around $x \approx 0.5$ and is followed by a maximum in the temperature dependence of the normalized resistivity and a decrease for low temperatures. In the inset we show the peak for $LaSb_2$ and for $La_{0.9}Ce_{0.1}Sb_2$ close to room temperature. Remarkably, the CDW transition increases above room temperature and is still visible as a kink at 355 K in pure $LaSb_2$.

We summarize results in the phase diagram shown in Fig. 6. In the upper panel we show the evolution of the CDW onset temperature with x and schematically highlight the size of the kink in the resistivity by a gradient in the wine color background. We estimate the size of the kink vs x by calculating the increase in the normalized resistance minus the resistance of the pure $CeSb_2$ compound, $\Delta\rho_{CDW} = (\frac{R(T_0)}{R_{300\,K}})_x - (\frac{R(T_0)}{R_{300\,K}})_{x=1}$ (with R being the resistance and T_0 the

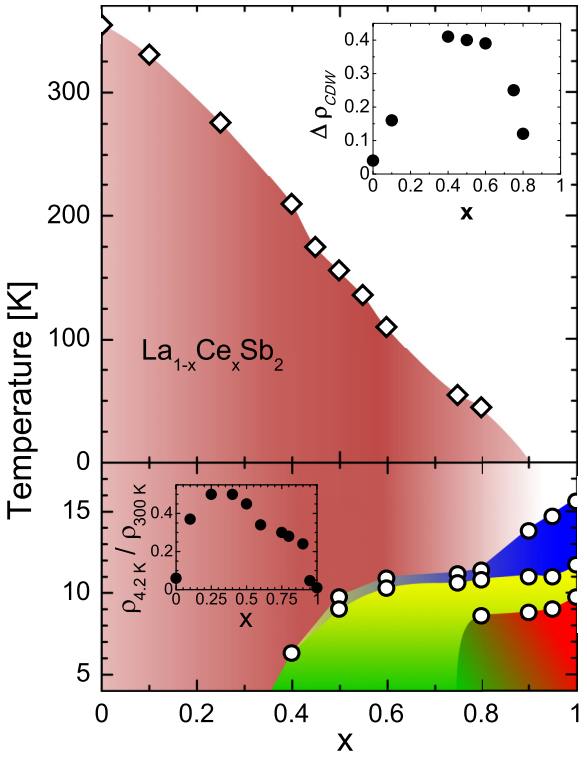

FIG. 6. (Color online) Phase diagram as obtained from anomalies observed in the resistivity and specific heat of the $La_{1-x}Ce_xSb_2$ series. CDW order is represented in the top panel. For both main panels, the intensity of the colored background (wine color) schematically represents the size of the jump in the resistive CDW transition. This is more pronounced for intermediate concentrations. Magnetic transitions are shown in the lower panel, with the different phases in different colors. In the upper right inset of the upper panel we show the size of the jump in the resistive CDW transition, as obtained from the normalized resistances minus the resistance of pure $CeSb_2$, i.e., $\Delta\rho_{\rm CDW} = (\frac{R(T_0)}{R_{300\,\rm K}})_x - (\frac{R(T_0)}{R_{300\,K}})_{x=1}$ (R being the resistance and T_0 the temperature where we find the CDW induced maximum in resistance for $x < 0.8$), vs. x. In the inset of the lower panel we show the inverse of the residual resistance ratio vs. x.

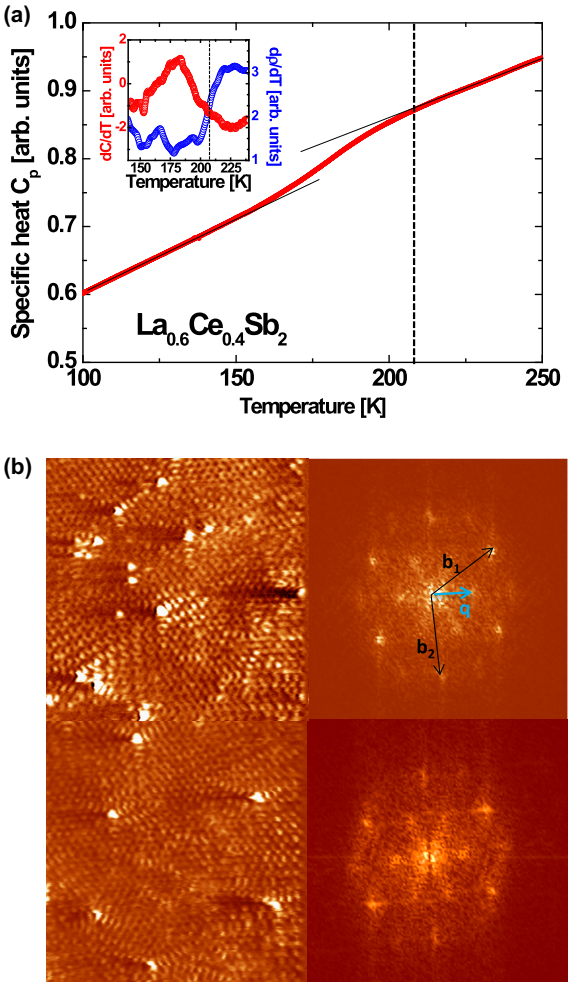

FIG. 7. (Color online) In (a) we show the specific heat C_P vs. temperature of a sample of $La_{0.6}Ce_{0.4}Sb_2$. Lines following the data points (red) are guides to the eye. In the inset we show the temperature derivatives of specific heat $\frac{dC_P}{dT}$ and resistivity $\frac{d\rho}{dT}$. We observe a broad transition starting at approximately 210 K (vertical dashed lines in the inset and in the figure). In (b) we show STM experiments on a sample with the same x. On the left we show two STM images and their corresponding Fourier transforms taken at 77 K. The observed wave vectors at the Fourier transform images correspond to reciprocal space vectors $b_i = 2 \cdot \pi / a_i$ of lengths $b_1 = 10.7\,\text{nm}^{-1}$ and $b_2 = 10.4\,\text{nm}^{-1}$, respectively. The lateral size of the real-space image is of 18 nm. An additional modulation is observed at an angle of roughly 30° to b_1,b_2 with wave vector q of approximately 5 nm^{-1} size.

temperature where we find the CDW induced maximum in resistance for $x < 0.8$). The result is shown in the inset in Fig. 6 (top panel). The size of the feature in the resistivity due to the CDW has a peak at intermediate concentrations x. In the bottom panel of Fig. 6, we show the magnetic transitions.

The inverse of the residual resistance ratio ($1/RRR = \frac{\rho(4.2\text{ K})}{\rho(300\text{ K})}$) vs Ce concentration is plotted as an inset in the bottom panel of Fig. 6. It deviates slightly from the Nordheim rule for substitutional induced scattering in randomly mixed alloys [residual resistivity varies as $x(1-x)$] [34]. We observe, for small x, a rather strong increase in $1/RRR$ with Ce concentration. Above $x = 0.5$, when magnetic order sets in, we find a downturn of the resistivity vs temperature at low temperatures. Thus, the onset of magnetic ordering decreases magnetic scattering and the residual resistivity becomes smaller. It continues decreasing slightly to about $x = 0.9$ until it drops to the value of pure $CeSb_2$. Below $x < 0.5$, the CDW induced increase in the resistivity increases the residual value, which drops for small x when the CDW ordering temperature increases to room temperature and above.

Using STM and AC calorimetry experiments we have examined in more detail the CDW of the compound with $x = 0.4$ (Fig. 7). As shown in Fig. 7(a), the specific heat C_P shows an anomaly at the onset of CDW. The temperature derivatives of specific heat C_P and resistivity ρ are compared in the inset. At about 210 K, the transition sets in, with a rather broad anomaly continuing over a few tens of K. With STM experiments, we have observed up to 20 surfaces as those presented in Fig. 7(b). These show distorted tetragonal arrangements with wave vectors b_1 and b_2. The observed vector size is compatible with in-plane lattice wave vectors of 0.63 and 0.62 nm, of similar size as that found in x-ray scattering (see Appendix, Table I). In addition, we observe a charge

modulation of larger wavelength with the main wave vector at 30° to the atomic lattice [marked with a blue arrow in Fig. 7(b)].

IV. DISCUSSION AND CONCLUSIONS

CDWs appear in many quasi-two-dimensional compounds with in-plane square atomic arrangements, such as tellurides, silicides, and compounds related to the cuprate superconductors, such as La_2NiO_4 [35,36]. Generally, CDWs can influence the electronic properties of materials resulting in very different ground states. For instance, a CDW can be accompanied by a metal-to-insulator transition or be connected to low-temperature superconductivity [37,38]. Other materials with a CDW are the transition-metal dichalcogenides such as $2H-NbSe_2$ and related compounds [38–41]. These have a layered hexagonal structure. Generally dopants or substitution decrease the CDW ordering temperature. At the same time, the CDW features observed in the experiments are smeared by substitution [35,42]. For instance, in the series $La_{1-x}Ce_xAgSb_2$ a decrease in T_{CDW} of about 5 K per percentage concentration of Ce is found. At the same time, the feature in resistivity is smeared by substitution. CDW is no longer found for $x = 0.3$.

By contrast, here in $La_{1-x}Ce_xSb_2$ we find that the CDW transition is found in nearly the whole series. T_{CDW} in $LaSb_2$ is above room temperature and the decrease is of about 3 K per percentage concentration of Ce. Most notably, the feature in the resistivity produced by CDW ordering becomes larger with increasing x and peaks at about $x = 0.5$. Thus, in the $La_{1-x}Ce_xSb_2$ series, substitutional disorder leads to a better defined CDW transition. Substitution of La by Ce, the minimal distortion of the pure compounds one can think of [43], stabilizes the CDW.

Generally it is considered that disorder plays against the formation of static CDWs because the Fermi surface is smeared by scattering. However, dynamic, or fluctuating, CDWs can be pinned by disorder [36,44–46]. Condensation of CDW by disorder has been examined in Refs. [35,36,44–49]. Pinning of the CDW bears some similarities to pinning of the vortex lattice in superconductors [50–52], and is discussed using the Fukuyama-Lee-Rice theory [53,54]. As in the vortex lattice, there are two competing energies [35,55]. The interaction between CDW and pinning sites is due to the modification of magnitude, wavelength, and phase of the CDW from electronic scattering at the pinning centers. There is a decrease in energy from the CDW adapting to the pinning centers and an increase due to the cost in long-range coherence for the whole CDW. Stacking faults or other defects can give pointlike pinning of CDW, whereas coupling to the random substitutional disorder can give collective pinning. Thus, $La_{1-x}Ce_xSb_2$ shows weak or fluctuating charge order, probably caused by strong electron-electron or electron-phonon correlations, that is stabilized by the interaction between the CDW and the random potential produced by disorder.

The possibility of a CDW in $LaSb_2$ (not confirmed until this work) has been discussed in the past to the positive and large magnetoresistance observed in this compound. Similarly large magnetoresistances are found in RSb_2 with R = Pr and Nd, as well as in $LaAgSb_2$. Alternative possible explanations of large magnetoresistances included disorder or Dirac band dispersion relations. The low residual resistivity of $LaSb_2$ rules out disorder-related effects [10,17]. The electron density of $LaSb_2$ has been reported to be of 3×10^{20} cm^{-3}, which is relatively low, yet higher than in typical semimetals [3]. Dirac-like excitations [11,12,15] have not been found until now in Fermi-surface measurements such as quantum oscillations or photoemission [2,5,56]. Thus, the available feature to explain the linear magnetoresistance in $LaSb_2$ is the CDW transition found here. The positive magnetoresistance is absent when substituting La with Ce and only appears in $LaSb_2$, when the CDW feature in resistivity is weakest and has the highest T_{CDW}. This shows that the substitutional disorder enhances the CDW feature but eliminates the linear magnetoresistance.

TABLE I. Refined lattice parameters, atomic positions, and atomic displacement parameters of $La_{1-x}Ce_xSb_2$ ($x = 0$, 0.4, 0.6 and 1) in orthorhombic *Cmca*(#64) at 80 and 300 K. The La[Ce] and Sb1 atoms were located at the 8*f* Wyckoff sites and the Sb2 at the 8*e* Wyckoff sites of *Cmca*. Agreement factors (R_{Bragg} and R_{wp}) are also given.

$La_{1-x}Ce_xSb_2$		$x = 0$		$x = 0.4$		$x = 0.6$		$x = 1$	
T (K)		80	300	80	300	80	300	80	300
a (Å)		6.3187(3)	6.33483(17)	6.3038(2)	6.31942(14)	6.290(7)	6.3110(8)	6.27043(16)	6.28709(15)
b (Å)		6.2001(3)	6.2128(2)	6.1838(2)	6.19828(16)	6.1681(6)	6.1878(6)	6.15017(13)	6.16676(13)
c (Å)		18.5403(6)	18.5500(4)	18.4182(7)	18.4242(6)	18.321(2)	18.3506(17)	18.2126(3)	18.2425(3)
V (Å^3)		726.34(5)	730.08(3)	717.96(4)	721.67(3)	710.81(12)	716.62(13)	702.35(3)	707.28(3)
La[Ce](8*f*)	y/b	0.402(3)	0.396(3)	0.384(4)	0.382(4)	0.367(4)	0.368(5)	0.373(2)	0.373(3)
	z/c	0.4027(6)	0.3998(6)	0.3976(6)	0.3992(5)	0.3993(7)	0.4003(7)	0.3973(4)	0.3948(5)
	U_{iso} (Å^2)	0.077(4)	0.081(5)	0.072(5)	0.095(5)	0.1344(8)	0.163(4)	0.0794(0)	0.094(5)
Sb1(8*f*)	y/b	0.886(4)	0.889(4)	0.884(4)	0.877(3)	0.865(6)	0.864(7)	0.862(3)	0.866(3)
	z/c	0.4286(6)	0.4301(6)	0.4283(6)	0.4263(4)	0.4270(6)	0.4276(7)	0.4311(5)	0.4296(5)
	U_{iso} (Å^2)	0.092(6)	0.103(6)	0.069(5)	0.057(3)	0.1116(8)	0.159(4)	0.0915(1)	0.072(4)
Sb2(8*e*)	y/b	0.132(4)	0.140(4)	0.1320(7)	0.127(2)	0.1105(6)	0.1129(8)	0.107(2)	0.1028(2)
	U_{iso} (Å^2)	0.067(4)	0.057(4)	0.047(3)	0.069(3)	0.1148(6)	0.143(3)	0.046(2)	0.048(2)
R_{Bragg} (%)		6.82	6.39	11.4	6.03	7.44	10.1	5.69	5.54
R_{wp} (%)		8.81	7.55	13.3	10.2	10.2	9.87	7.41	7.11

It is interesting to discuss the hybridization of the Ce ion and the magnetic interactions by comparison with $La_{1-x}Ce_xAgSb_2$. In $La_{1-x}Ce_xAgSb_2$, there is a small Kondo increase of the resistance at low temperatures. Instead, in $La_{1-x}Ce_xSb_2$, we observe the gradual appearance of the magnetic transitions of $CeSb_2$. These transitions are likely caused by Ruderman-Kittel-Kasuya-Yosida (RKKY) interactions [1,2]. Thus, the two systems $La_{1-x}Ce_xSb_2$ and $La_{1-x}Ce_xAgSb_2$ feature the two opposing effects of the Ce ions, either RKKY induced local moment ordering or Kondo hybridization. The decrease of T_{CDW} together with the establishment of well-developed magnetic transitions for large x in $La_{1-x}Ce_xSb_2$ suggests that CDW and magnetism compete for the same kind of electron-electron interactions.

Finally, regarding superconductivity, let us note that the influence of CDWs on superconductivity has been discussed in the cuprates to some extent [57–59]. It has been argued that fluctuating CDWs can coexist with high-T_C superconductivity, whereas static CDW has a tendency to compete with superconducting correlations [60]. The relationship with magnetic fluctuations has also been extensively discussed, but the observed differences in wave vectors and directions have not yet been reconciled [44,61]. Anomalous and inhomogeneous superconducting densities of states are ubiquitously found in many cuprates [62–64]. Our results suggest that the anomalous properties of superconductivity in $LaSb_2$, such as the broad resistive transitions and increased Fermi-level density of states in the superconducting phase, could be related to the presence of the CDW.

In summary, we have studied the system $La_{1-x}Ce_xSb_2$ and obtained the variation of resistivity and lattice parameters with x. We have shown that a CDW appears in $LaSb_2$ and that it becomes more pronounced when substituting La by Ce at a balanced mixture between both elements.

ACKNOWLEDGMENTS

We acknowledge P. C. Canfield for helping us to set up our growth laboratory and teaching us details about solution growth. E.H. acknowledges the support of Departamento Administrativo de Ciencia, Tecnología e Innovación, COLCIENCIAS (Colombia) Programa Doctorados en el Exterior Convocatoria 568-2012. This work was supported by the Spanish MINECO (FIS2014-54498-R, MAT2011-27470-C02-02, and CSD-2009-00013), by the European Union (Graphene Flagship Contract No. CNECT-ICT-604391 and COST MP1201 action), and by the Comunidad de Madrid through programs Nanofrontmag-CM (S2013/MIT-2850) and MAD2D-CM (S2013/MIT-3007). We acknowledge MINECO and CSIC for financial support and for provision of synchrotron radiation facilities and would like to thank the SpLine BM25 staff for assistance in using the beamline. We acknowledge technical support of UAM's workshops, SEGAINVEX.

APPENDIX

Here we provide the details of Rietveld refinement. In Fig. 8 we show the x-ray powder diffraction data and compare the results with expectations for the $La_{1-x}Ce_xSb_2$ series and for pure Sb, used as a flux during crystal growth. The amount of Sb is <10 wt. % in all samples. In Table I we provide

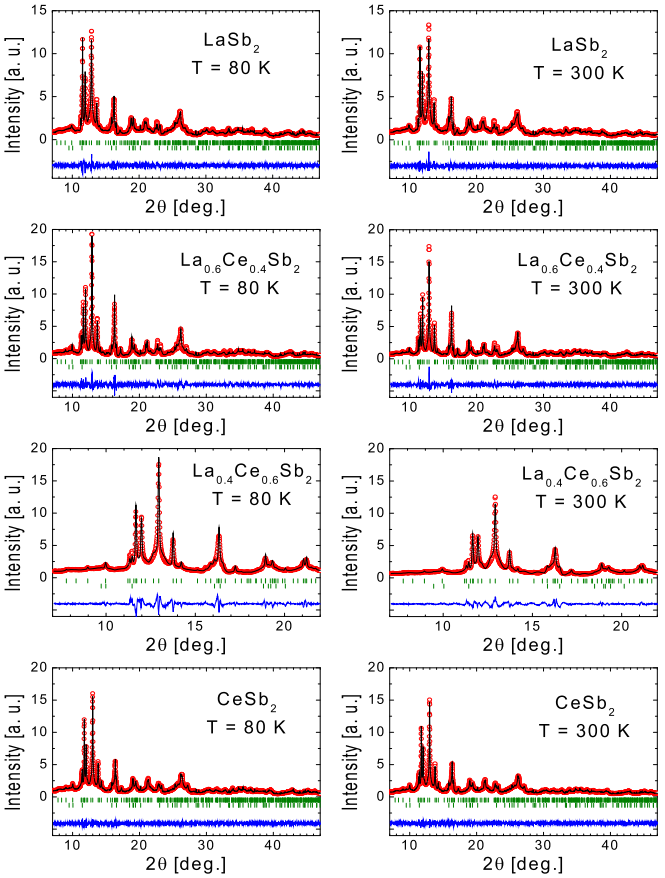

FIG. 8. (Color online) Observed (red circles), calculated (solid black line) and difference (lower solid blue line) XRPD ($\lambda = 0.621$ Å) profiles of $La_{1-x}Ce_xSb_2$ for $x = 0$, 0.4, 0.6 and 1 at 80 and 300 K. Green ticks indicate the position of allowed reflections in $La_{1-x}Ce_xSb_2$-*Cmca* (upper) and Sb-$R\bar{3}m$ (lower).

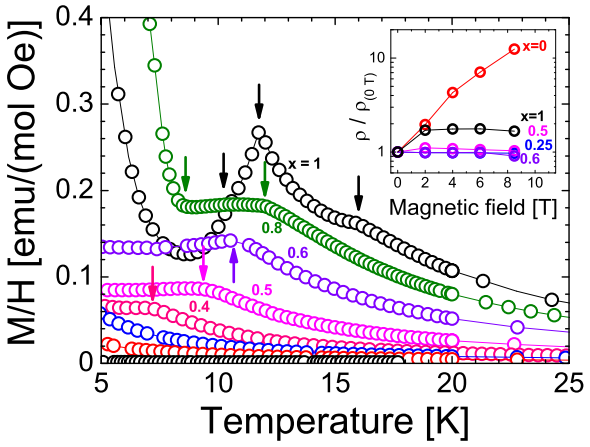

FIG. 9. (Color online) The magnetization vs. temperature in the $La_{1-x}Ce_xSb_2$ series taken in a Quantum Design SQUID magnetometer at 1 kOe. Concentrations x are provided as numbers. Arrows show the phase transition points plotted in the phase diagram of Fig. 6. Curves not marked with numbers give the results for nonmagnetic concentrations for $x < 0.4$, namely, 0.25, 0.1, and pure $LaSb_2$. In the inset we show the resistivity vs. magnetic field at 2 K for a few values of x.

the lattice parameters for four different concentrations. To compare with STM experiments (Fig. 7) we have transformed the wave vectors b_1 and b_2 in the publication to an orthogonal base $a = A_1$ and $b = A_1 + 2 \times A_2$ with A_1 and A_2 being the real-space atomic distances corresponding to reciprocal space wave vectors b_1 and b_2. We obtain $a = 0.63$ nm and $b = 2 \times 0.62$ nm, compatible with data shown in Table I.

We also provide the magnetization vs. temperature for the samples showing a magnetic transition in Fig. 9. The peaks and kinks observed in these measurements are used to build up the magnetic phase diagram of Fig. 6. In the inset of Fig. 9 we show the resistivity vs. magnetic field at 2 K. Note the disappearance of strong variations of the resistivity with the magnetic field at a finite x.

[1] P. C. Canfield, J. Thompson, and Z. Fisk, Novel Ce magnetism in Ce Dipnictide and Di-Ce pnictide structures, J. Appl. Phys. **70**, 5992 (1991).

[2] S. L. Bud'ko, P. C. Canfield, C. H. Mielke, and A. H. Lacerda, Anisotropic magnetic properties of light rare-earth diantimonides, Phys. Rev. B **57**, 13624 (1998).

[3] D. P. Young, R. G. Goodrich, J. F. DiTusa, S. Guo, P. W. Adams, J. Y. Chan, and D. Hall, High Magnetic Field Sensor Using $LaSb_2$, Appl. Phys. Lett. **82**, 3713 (2003).

[4] J. A. Galvis, H. Suderow, S. Vieira, S. L. Bud'ko, and P. C. Canfield, Scanning tunneling microscopy in the superconductor $LaSb_2$, Phys. Rev. B **87**, 214504 (2013).

[5] A. I. Acatrinei, D. Browne, Y. B. Losovyi, D. P. Young, M. Moldovan, J. Y. Chan, P. T. Sprunger, and R. L. Kurtz, Angle-resolved photoemission study and first-principles calculation of the electronic structure of $LaSb_2$, J. Phys.: Condens. Matter **15**, L511 (2003).

[6] F. Hulliger and H. R. Ott, Superconductivity of lanthanum pnictides, J. Less-Common Met. **55**, 103 (1977).

[7] S. Guo, D. P. Young, P. W. Adams, X. S. Wu, J. Y. Chan, G. T. McCandless, and J. F. DiTusa, Dimensional crossover in the electrical and magnetic properties of the layered $LaSb_2$ superconductor under pressure: The role of phase fluctuations, Phys. Rev. B **83**, 174520 (2011).

[8] A. A. Abrikosov, Quantum magnetoresistance of layered semimetals, Phys. Rev. B **60**, 4231 (1999).

[9] A. E. Koshelev, Linear magnetoconductivity in multiband spin-density-wave metals with nonideal nesting, Phys. Rev. B **88**, 060412 (2013).

[10] M. M. Parish and P. B. Littlewood, Non-saturating magnetoresistance in heavily disordered semiconductors, Nature (London) **426**, 162 (2003).

[11] D. -X. Qu, Y. S. Hor, J. Xiong, R. J. Cava, and N. P. Ong, Quantum oscillations and Hall anomaly of surface states in the topological insulator Bi_2Te_3, Science **329**, 821 (2010).

[12] F. Y. Yang, K. Liu, K. Hong, D. H. Reich, P. C. Searson, and C. L. Chien, Large magnetoresistance of electrodeposited single-crystal bismuth thin films, Science **284**, 1335 (1999).

[13] A. H. Castro Neto, F. Guinea, N. M. R. Peres, K. S. Novoselov, and A. K. Geim, The electronic properties of graphene, Rev. Mod. Phys. **81**, 109 (2009).

[14] F. Muñoz-Rojas, J. Fernández-Rossier, and J. J. Palacios, Giant Magnetoresistance in Ultrasmall Graphene Based Devices, Phys. Rev. Lett. **102**, 136810 (2009).

[15] A. Narayanan, M. D. Watson, S. F. Blake, N. Bruyant, L. Drigo, Y. L. Chen, D. Prabhakaran, B. Yan, C. Felser, T. Kong, P. C. Canfield, and A. I. Coldea, Linear Magnetoresistance Caused by Mobility Fluctuations in n-Doped Cd_3As_2, Phys. Rev. Lett. **114**, 117201 (2015).

[16] A. A. Abrikosov, Quantum magnetoresistance, Phys. Rev. B **58**, 2788 (1998).

[17] J. C. W. Song, G. Refael, and P. A. Lee, Guiding center linear magnetoresistance in the semiclassical regime, Phys. Rev. B **92**, 180204(R) (2015).

[18] L. M. Falicov and H. Smith, Linear Magnetoresistance and Anisotropic Quantum Fluctuations, Phys. Rev. Lett. **29**, 124 (1972).

[19] M. Naito and S. Tanaka, Galvanomagnetic effects in the charge-density-wave state of $2H - NbSe_2$ and $2H - TaSe_2$, J. Phys. Soc. Jpn. **51**, 228 (1982).

[20] E. Mun, S. L. Bud'ko, and P. C. Canfield, Thermoelectric power of $RAgSb_2$ (R = Y, La, Ce, and Dy) in zero and applied magnetic fields, J. Phys.: Condens. Matter **23**, 476001 (2011).

[21] K. D. Myers, S. L. Bud'ko, I. R. Fisher, Z. Islam, H. Kleinke, A. H. Lacerda, and P. C. Canfield, Systematic study of anisotropic transport and magnetic properties of $RAgSb_2$ (R = Y, La-Nd, Sm, Gd-Tm), J. Magn. Magn. Mater. **205**, 27 (1999).

[22] C. Song, J. Park, J. Koo, K. -B. Lee, J. Y. Rhee, S. L. Bud'ko, P. C. Canfield, B. N. Harmon, and A. I. Goldman, Charge-density-wave orderings in $LaAgSb_2$: An x-ray scattering study, Phys. Rev. B **68**, 035113 (2003).

[23] S. L. Bud'ko and P. C. Canfield, Magnetism and superconductivity in rare earth-nickel-borocarbides, C. R. Physique **7**, 56 (2006).

[24] M. S. Torikachvili, S. L. Bud'ko, S. A. Law, M. E. Tillman, E. D. Mun, and P. C. Canfield, Hydrostatic pressure study of pure and doped $La_{1-x}R_xAgSb_2$ (R = Ce, Nd) charge-density-wave compounds, Phys. Rev. B **76**, 235110 (2007).

[25] P. C. Canfield, *Solution Growth of Intermetallic Single Crystals: A Beginner's Guide*, Book Series on Complex Metallic Alloys, Vol. 2, edited by E. Belin-Ferré (World Scientific, Singapore, 2007).

[26] P. C. Canfield and Z. Fisk, Growth of single crystals from metallic fluxes, Philos. Mag. Lett. Part B **65**, 1117 (1992).

[27] Materials Preparation Center, Ames Laboratory U.S. DOE Basic Energy Sciences, Ames, IA, USA, available from: www.mpc.ameslab.gov.

[28] J. Rodríguez-Carvajal, Recent advances in magnetic structure determination by neutron powder diffraction, Physica B **192**, 55 (1993).

[29] P. Villars and L. Calvert, *Pearson's Handbook of Crystallographic Data for Intermetallic Phases* (ASM International, Materials Park, OH, 1991), Vol. 4.

[30] T. Pérez-Castañeda, J. Azpeitia, J. Hanko, A. Fente, H. Suderow, and M. A. Ramos, Low-temperature specific heat of graphite and $CeSb_2$: Validation of a quasi-adiabatic continuous method, J. Low. Temp. Phys. **173**, 4 (2013).

[31] H. Suderow, I. Guillamon, and S. Vieira, Compact very low temperature scanning tunneling microscope with mechanically driven horizontal linear positioning stage, Rev. Sci. Instrum. **82**, 033711 (2011).

[32] A. Fente, I. Guillamon, S. Ran, S. Vieira, H. Suderow, S. L. Budko, and P. C. Canfield, Observation of unreconstructed square atomic square lattice in $Ca(Fe_{0.965}Co_{0.035})_2As_2$ cleaved at very low temperatures, J. Phys.: Conf. Ser. **568**, 022046 (2014).

[33] N. L. Eatough and H. T. Hall, High-pressure synthesis of rare earth diantimonides, Inorg. Chem. **8**, 1439 (1969).

[34] L. Nordheim, Zur elektronentheorie der metalle. I, Ann. Phys. (NY) **401**, 607 (1931).

[35] P. Monceau, Electronic crystals: An experimental overview, Adv. Phys. **61**, 325 (2012).

[36] J. M. Tranquada, B. J. Sternlieb, J. D. Axe, Y. Nakamura, and S. Uchida, Evidence for stripe correlations of spins and holes in copper oxide superconductors, Nature (London) **375**, 561 (1995).

[37] X. Zhang, J. Li, B. Foran, S. Lee, H. -Y. Guo, T. Hogan, C. R. Kannewurf, and M. G. Kanatzidis, Distorted square nets of tellurium in the novel quaternary polytelluride $K_{0.33}Ba_{0.67}AgTe_2$, J. Am. Chem. Soc. **117**, 10513 (1995).

[38] I. Guillamón, H. Suderow, S. Vieira, L. Cario, P. Diener, and P. Rodiere, Superconducting Density of States and Vortex Cores of 2H − $NbSe_2$, Phys. Rev. Lett. **101**, 166407 (2008).

[39] M. D. Johannes, I. I. Mazin, and C. A. Howells, Fermi-surface nesting and the origin of the charge-density wave in $NbSe_2$, Phys. Rev. B **73**, 205102 (2006).

[40] J. D. Fletcher, A. Carrington, P. Diener, P. Rodiére, J. P. Brison, R. Prozorov, T. Olheiser, and R. W. Gianetta, Penetration Depth Study of Superconducting Gap Structure of 2H − $NbSe_2$, Phys. Rev. Lett. **98**, 057003 (2007).

[41] C. D. Malliakas and M. G. Kanatzidis, NbNb interactions define the charge density wave structure of 2H − $NbSe_2$, J. Am. Chem. Soc. **135**, 1719 (2013).

[42] G. Gómez-Santos and F. Ynduráin, Effects of impurities on charge-density waves: A mean-field calculation, Phys. Rev. B **29**, 4459 (1984).

[43] H. Hodovanets, S. L. Bud'ko, W. E. Straszheim, V. Taufour, E. D. Mun, H. Kim, R. Flint, and P. C. Canfield, Remarkably Robust and Correlated Coherence and Antiferromagnetism in $(Ce_{1-x}La_x)Cu_2Ge_2$, Phys. Rev. Lett. **114**, 236601 (2014).

[44] H.-H. Klauss, W. Wagener, M. Hillberg, W. Kopman, H. Walf, F. J. Litterst, M. Hücker, and B. Büchner, From Antiferromagnetic Order to Static Magnetic Stripes: The Phase Diagram of $(La,Eu)_{2-x}Sr_xCuO_4$, Phys. Rev. Lett. **85**, 4590 (2000).

[45] J. I. Okamoto, C. J. Arguello, E. P. Rosenthal, A. N. Pasupathy, and A. J. Millis, Experimental Evidence for a Bragg Glass Density Wave Phase in a Transition-Metal Dichalcogenide, Phys. Rev. Lett. **114**, 026802 (2015).

[46] C. J. Arguello, S. P. Chockalingam, E. P. Rosenthal, L. Zhao, C. Gutierrez, J. H. Kang, W. C. Chung, R. M. Fernandes, S. Jia, A. J. Millis, R. J. Cava, and A. N. Pasupathy, Visualizing the charge density wave transition in 2H − $NbSe_2$ in real space, Phys. Rev. B **89**, 235115 (2014).

[47] S. Ravy, S. Rouziere, J. P. Pouget, S. Brazovskii, J. Marcus, J. F. Bérar, and E. Elkaim, Disorder effects on the charge-density waves structure in V- and W-doped blue bronzes: Friedel oscillations and charge-density wave pinning, Phys. Rev. B **74**, 174102 (2006).

[48] Y. Feng, J. Wang, R. Jaramillo, J. van Wezel, S. Haravifard, G. Srajer, Y. Liu, Z.-A. Xu, P. B. Littlewood, and T. F. Rosenbaum, Order parameter fluctuations at a buried quantum critical point, Proc. Natl. Acad. Sci. USA **109**, 7224 (2012).

[49] H. H. Weitering, J. M. Carpinell, A. V. Melechko, J. Zhang, M. Bartkowiak, and E. W. Plummer, Defect-mediated condensation of a charge density wave, Science **285**, 2107 (1999).

[50] G. Blatter, M. V. Feigel'man, V. B. Geshkenbein, A. I. Larkin, and V. M. Vinokur, Vortices in high-temperature superconductors, Rev. Mod. Phys. **66**, 1125 (1994).

[51] E. H. Brandt, Tilted and curved vortices in anisotropic superconducting films, Phys. Rev. B **48**, 6699 (1993).

[52] H. Suderow, I. Guillamón, J. G. Rodrigo, and S. Vieira, Imaging superconducting vortex cores and lattices with a scanning tunneling microscope, Supercond. Sci. Technol. **27**, 063001 (2014).

[53] H. Fukuyama and P. A. Lee, Dynamics of the charge-density wave. I. Impurity pinning in a single chain, Phys. Rev. B **17**, 535 (1978).

[54] P. A. Lee and T. M. Rice, Electric field depinning of charge density waves, Phys. Rev. B **19**, 3970 (1979).

[55] W. Aichmann, Individual pinning of CDW phase: Beyond the Born approximation, Phys. B: Condens. Matter **217**, 8 (1996).

[56] R. G. Goodrich, D. Browne, R. Kurtz, D. P. Young, J. F. DiTusa, P. W. Adams, and D. Hall, de Haas–van Alphen measurements of the electronic structure of $LaSb_2$, Phys. Rev. B **69**, 125114 (2004).

[57] C. V. Parker, P. Aynajian, E. H. da Silva Neto, A. Pushp, S. Ono, J. Wen, Z. Xu, G. Gu, and A. Yazdani, Fluctuating stripes at the onset of the pseudogap in the high-T_c superconductor $Bi_2Sr_2CaCu_2O_{8+x}$, Nature (London) **468**, 677 (2010).

[58] E. H. da Silva Neto, P. Aynajian, A. Frano, R. Comin, E. Schierle, E. Weschke, A. Gyenis, J. Wen, J. Schneeloch, Z. Xu, S. Ono, G. Gu, M. Le Tacon, and A. Yazdani, Ubiquitous interplay between charge ordering and high-temperature superconductivity in cuprates, Science **343**, 393 (2013).

[59] G. Ghiringhelli, M. Le Tacon, M. Minola, S. Blanco-Canosa, C. Mazzoli, N. B. Brookes, G. M. De Luca, A. Frano, D. G. Hawthorn, F. He, T. Loewe, M. Moretti Sala, D. C. Peets, M. Salluzzo, E. Schierle, R. Sutarto, G. A. Sawatzky, E. Weschke, B. Keimer, and L. Braikovich, Long-range incommensurate charge fluctuations in $(Y,Nd)Ba_2Cu_3O_{6+x}$, Science **337**, 821 (2012).

[60] D. H Torchinsky, F. Mahmood, A. T Bollinger, I. Bozovic, and N. Gedik, Fluctuating charge-density waves in a cuprate superconductor, Nat. Mater. **12**, 387 (2013).

[61] S. A. Kivelson, I. P. Bindloss, E. Fradkin, V. Oganesyan, J. M. Tranquada, A. Kapitulnik, and C. Howald, How to detect fluctuating stripes in the high-temperature superconductors, Rev. Mod. Phys. **75**, 1201 (2003).

[62] O. Fischer, M. Kugler, I. Maggio-Aprile, C. Berthod, and C. Renner, Scanning tunneling spectroscopy of high-temperature superconductors, Rev. Mod. Phys. **79**, 353 (2007).

[63] J. R. Kirtley, Tunneling measurements of the energy gap in high-T_c superconductors, Int. J. Mod. Phys. B **04**, 201 (1990).

[64] J. E. Hoffman, E. W. Hudson, K. M. Lang, V. Madhavan, H. Eisaki, S. Uchida, and J. C. Davis, A four unit cell periodic pattern of quasi-particle states surrounding vortex cores in $Bi_2Sr_2CaCu_2O_{8+\delta}$, Science **295**, 466 (2002).